INTERIOR IMPEDANCE WEDGE DIFFRACTION WITH SURFACE WAVES

Semiannual Report

Constantine A. Balanis and Timothy Griesser
August 1, 1987 - January 31, 1988

Department of Electrical and Computer Engineering
Arizona State University
Tempe, AZ 85287

Grant No. NAG-1-562
National Aeronautics and Space Administration
Langley Research Center
Hampton, VA 23665

ABSTRACT

The exact impedance wedge solution is evaluated asymptotically using the method of steepest descents for plane wave illumination at normal incidence. Uniform but different impedances on each face are considered for both soft and hard polarizations. The asymptotic solution isolates the incident, singly reflected, multiply reflected, diffracted, and surface wave fields. Multiply reflected fields of any order are permitted. The multiply reflected fields from the exact solution are written as ratios of auxiliary Maliuzhinets functions, whereas a geometrical analysis gives the reflected fields as products of reflection coefficients. These two representations are shown to be identical in magnitude, phase and the angular range over which they exist. The diffracted field includes four Fresnel transition functions as in the perfect conductor case, and expressions for the appropriate discontinuities at the shadow boundaries are presented. The surface wave exists over a finite angular range and only for certain surface impedances. A surface wave transition field is included to retain continuity. Computations are presented for interior wedge diffractions although the formulation is valid for both exterior and interior wedges.

I. INTRODUCTION

During this six-month reporting period, our efforts have primarily concentrated in deriving diffraction functions to predict the fields diffracted by an interior wedge with impedance surfaces. Such diffraction functions are most important in analyzing the scattering patterns of impedance surfaces, such as corner reflectors, with interior angles. Preliminary commputations of scattering patterns from such wedges are included in this report.

The impedance boundary condition has been widely used to analyze electromagnetic problems for which the material properties or surface characteristics are important. The boundary condition is often appropriate for lossy or layered material or for statistically rough surfaces, and it provides an approximate means whereby reflection, diffraction and surface wave phenomena on physical structures can be studied. The impedance boundary condition is a useful approximation for many physical problems because it includes the material effects without explicitly involving the fields within the material.

The exact solution for diffraction from an impedance wedge was presented by Maliuzhinets [1]-[2] for the case of uniform but different impedances on each face and for normal incidence. Bucci and Franceschetti [3] considered both normal and oblique incidence on the half plane and presented a more detailed analysis of the surface wave contribution. Tiberio, Pelosi and Manara [4] performed a uniform GTD asymptotic evaluation of the exact solution for the exterior impedance wedge. Herman and Volakis [5] presented an alternative steepest descent

GTD evaluation for the exterior wedge and also included surface wave terms.

In this paper, a uniform geometrical theory of diffraction with surface wave contributions is presented for the interior wedge. This extends the applicability of the present theory to allow solution of more complex scattering geometries which include interior wedges. Both exterior and interior wedge-like corners exist on many physical structures such as ships, aircraft or spacecraft. In addition, the faces of these interior wedges may be of different impedances. On a ship for example, the hull and the water surface form an interior wedge-like corner with faces of two different materials, namely water and steel. Other interior wedges exist between the deck and the superstructure of a ship or between the wing and fuselage of an airplane.

In this paper, the exact solution of Maliuzhinets is asymptotically evaluated using the method of steepest descents. This decomposes the exact integral solution into individual scattering mechanisms. The terms extracted include the incident field, the singly reflected fields, the multiply reflected fields, the diffracted field, the surface waves and the associated surface wave transition fields. The incident and reflected components of the geometrical optics solution are found in terms of the Maliuzhinets function as the residues of the geometrical optics poles. Each pole in the exact integral solution is shown to correspond to a particular geometrical optics term, and the residue of the pole is shown to be equivalent to a product of reflection coefficients and a phase factor. Hence the steepest descent solution

extracts reflection terms which can be found directly in terms of reflection coefficients on impedance surfaces. This correspondence of the residues and the reflection coefficients has been demonstrated only for the singly reflected fields for the half plane [3], [6] and the exterior wedge [4]. The pole residue reflection terms agree with the geometrical analysis in magnitude, phase and in the angular range over which the reflection exists.

The diffracted field is determined using the modified Pauli-Clemmow method of steepest descents [8]-[9], and it considers the effects of the four poles nearest the steepest descent paths. This yields four Fresnel transition functions which provide continuity across the shadow boundaries. The formulation is analogous to the perfectly conducting case with the introduction of suitable multiplying factors which are related to the reflection coefficients. These factors assure that the discontinuity in the diffracted field will provide the proper continuity in the total field.

The surface wave terms are obtained from the residues of complex poles of the auxiliary Maliuzhinets function. Unlike the geometrical optics poles, the location of the surface wave pole depends on the properties of the wedge material and hence the surface wave only exists for certain impedances. In addition, the surface wave exists only over a finite angular range, and a discontinuity is encountered at the surface wave boundary. This is analogous to the discontinuity at the geometrical optics shadow boundary. A surface wave transition field is added to uniformly account for the effects of the surface wave pole near the steepest descent path. This transition field removes the

discontinuity at the surface wave boundary just as the diffracted field removes the geometrical optics discontinuities. The surface wave transition field includes a Fresnel transition function of complex argument which provides the proper discontinuity. The steepest descent evaluation near the surface wave pole utilizes the method of Felsen and Marcuvitz [10] for complex poles.

II. THE EXACT INTEGRAL REPRESENTATION

The canonical wedge structure of interest is shown in Fig. 1a. The wedge has two faces located at $\phi=0$ and $\phi=n\pi$, referred to as the 0 and n faces, respectively. An exterior wedge has values of n in the range of $1\leq n\leq 2$, while for an interior wedge $0<n<1$. The faces have uniform normalized surface impedances of η_0 and η_n, respectively. A plane wave is incident from the direction ϕ' and the observation point P is at a distance ρ from the edge of the wedge at an angle ϕ, where ϕ and ϕ' are both measured from the 0 face. Assuming an incident field U_0, the exact solution for the total field, including the incident and scattered components, is [1], [5]

$$U_t(\rho,\phi) = \frac{-U_0}{2n\pi j}\int_\gamma \frac{\Psi(\alpha+\frac{n\pi}{2}-\phi)}{\Psi(\frac{n\pi}{2}-\phi')} \times \frac{\sin(\frac{\phi'}{n})}{\cos(\frac{\alpha-\phi}{n})-\cos(\frac{\phi'}{n})} e^{jk\rho\cos\alpha}\, d\alpha \quad (1)$$

where γ is the contour shown in Fig. 1b. An $e^{j\omega t}$ time convention is assumed and suppressed. In (1) $\Psi(\alpha)$ is the auxiliary Maliuzhinets

function [1] and depends on the parameters n, θ_0 and θ_n. Both the E_z and H_z polarizations are included in this representation [7]. For the soft (TM, E_z) polarization

$$U_t(r,\phi) = E_z(r,\phi) \qquad \sin\theta_0 = \frac{1}{\eta_0} \qquad \sin\theta_n = \frac{1}{\eta_n} \tag{2}$$

whereas for the hard (TE, H_z) polarization

$$U_t(r,\phi) = H_z(r,\phi) \qquad \sin\theta_0 = \eta_0 \qquad \sin\theta_n = \eta_n \tag{3}$$

The contribution of the steepest descent paths SDP(π) and SDP($-\pi$), shown in Fig. 1b, are added to enclose a region of the complex α plane. The steepest descent path SDP(θ) is the path along which

$$\alpha_r = \cos^{-1}[1/\cosh(\alpha_i)]\ \mathrm{sgn}(\alpha_i) + \theta \tag{4}$$

where $\alpha=\alpha_r+j\alpha_i$ [11]. Since the integral around the closed path is proportional to the sum of the enclosed pole residues, the total field can be written as

$$U_t(\rho,\phi) = \tag{5}$$

$$\frac{U_0}{n} \sum_p \mathrm{Res}\left[\frac{\Psi(\alpha + \frac{n\pi}{2} - \phi)}{\Psi(\frac{n\pi}{2} - \phi')} \frac{\sin(\frac{\phi'}{n})}{\cos(\frac{\alpha-\phi}{n}) - \cos(\frac{\phi'}{n})} e^{jk\rho\cos\alpha}, \alpha_p\right]$$

$$+ \frac{U_0}{2n\pi j} \int_{SDP} \frac{\Psi(\alpha + \frac{n\pi}{2} - \phi)}{\Psi(\frac{n\pi}{2} - \phi')} \frac{\sin(\frac{\phi'}{n})}{\cos(\frac{\alpha-\phi}{n}) - \cos(\frac{\phi'}{n})} e^{jk\rho\cos\alpha}\, d\alpha$$

where SDP is the path SDP(π) + SDP($-\pi$) and the α_p are the poles of the integrand. The notation Res[$f(\alpha),\alpha_p$] represents the residue of $f(\alpha)$ at the pole α_p.

The auxiliary Maliuzhinets function $\Psi(\alpha)$ can be written in terms

of the Maliuzhinets function $\Psi_n(\alpha)$ by [1], [4]

$$\Psi(\alpha) = \Psi_n(\alpha + \frac{n\pi}{2} + \frac{\pi}{2} - \theta_0)\Psi_n(\alpha + \frac{n\pi}{2} - \frac{\pi}{2} + \theta_0) \tag{6}$$

$$\cdot \Psi_n(\alpha - \frac{n\pi}{2} + \frac{\pi}{2} - \theta_n)\Psi_n(\alpha - \frac{n\pi}{2} - \frac{\pi}{2} + \theta_n)$$

Following [4], the order of the Maliuzhinets function will be denoted by the edge parameter n rather than the half wedge angle $\Phi = \frac{n\pi}{2}$. The half angle Φ was more appropriate for Maliuzhinets choice of referencing ϕ and ϕ_0 to the open wedge bisector. The necessary properties of $\Psi_n(\alpha)$ used in this paper are [1], [5]

$$\frac{\Psi_n(\alpha + n\pi)}{\Psi_n(\alpha - n\pi)} = \cot \frac{1}{2}(\alpha + \frac{\pi}{2}) \tag{7}$$

$$\Psi_n(-\alpha) = \Psi_n(\alpha) \tag{8}$$

$$\Psi_n\left[\alpha \pm (n\pi + \frac{3\pi}{2})\right] = \pm\sin(\frac{\pi \pm \alpha}{2n}) \csc(\frac{\alpha}{2n}) \Psi_n(n\pi - \frac{\pi}{2} \pm \alpha) \tag{9}$$

III. THE GEOMETRICAL OPTICS TERMS

The simplest way to calculate multiply reflected fields within an interior wedge is to use a reflection coefficient approach in which the incident field is multiplied by a reflection coefficient at each reflection. In this section it is shown that the pole residues of the exact solution give identically the same geometrical optics field as the simple ray tracing model. Both methods give identical results in magnitude, phase and also in the angular range over which a particular reflection mechanism exists. This has been shown previously only for for singly reflected fields for the half plane [3], [6] and the exterior

wedge [4].

For a geometrical analysis of the multiply reflected fields, the incident field is multiplied by the appropriate reflection coefficients and phase factors. The surface impedance reflection coefficients, appropriate for infinite planar boundaries and plane wave incidence are

$$\Gamma_0(\varphi) = \frac{\sin \varphi - \sin \theta_0}{\sin \varphi + \sin \theta_0} \tag{10a}$$

$$\Gamma_n(\varphi) = \frac{\sin \varphi - \sin \theta_n}{\sin \varphi + \sin \theta_n} \tag{10b}$$

where φ is the angle of incidence measured from the planar surface to the incident ray.

In general, the geometrical optics reflected field for any multiply reflected component C can be written as

$$U_{GO}^{C} = U_0 \Gamma_{\Pi}(\phi', \theta_0, \theta_n)\, e^{+jk\rho\cos(\alpha_p)} \tag{11}$$

where $\Gamma_{\Pi}(\phi', \theta_0, \theta_n)$ is a product of reflection coefficients and α_p is a distance factor which yields the appropriate phase delay. The multiply reflected field is identified by a sequence of 0's and n's indicating the order of reflection. As an example, component 0n0n is the quadruple reflected field, incident on face 0, which in order reflects from face 0 to n to 0 to n.

In Table I, the terms $\Gamma_{\Pi}(\phi', \theta_0, \theta_n)$ and α_p are listed for reflection mechanisms of up to fourth order. In addition, the range over which these terms exist is listed, with the implied conditions that $0<\phi<n\pi$ and $0<\phi'<n\pi$. The number of terms presented is sufficient to identify the pattern by which the table can be extended. The ordering of this table has been chosen to correspond to the positions of the poles in the exact

solution.

When considering the exact solution, the geometrical optics poles must first be identified. The geometrical optics poles are those poles for which

$$\cos\left(\frac{\alpha_p - \phi}{n}\right) = \cos\left(\frac{\phi'}{n}\right) \tag{12}$$

The geometrical optics poles are

$$\alpha_p = \phi \pm \phi' + 2mn\pi = \beta^{\pm} + 2mn\pi \tag{13}$$

where m is an integer and $\beta^{\pm} = \phi \pm \phi'$. The poles occur in two sets of equally spaced poles corresponding to either the upper or lower sign. For each set, the spacing between poles is $2n\pi$. If ϕ' is considered to be fixed and if ϕ runs from 0 to $n\pi$, then the geometrical optics poles move from $\pm\phi' + 2mn\pi$ to $\pm\phi' + 2mn\pi + n\pi$. These pole loci are plotted in Fig. 2 for $\phi' = 30^\circ$ and an 85° interior corner. The movement of the poles with increasing ϕ is indicated by the arrows, and it is noted that a given pole can only move half the distance to the next pole of the same set. In addition, the surface wave poles are shown for $\eta_0=\eta_n=0.2 + j\ 0.8$ although they are not considered until a later section. A particular pole contributes to the exact integral solution only if it lies within the steepest descent paths, and hence it is possible to identify each pole with a specific reflection mechanism by the angular ranges of existence listed in Table I. The reflection component corresponding to each pole is labeled in Fig. 2. For each geometrical reflection, the appropriate values of β and m are listed in Table I.

From the exact solution, the contribution of the geometrical optics pole is $-2\pi j$ times the residue of the pole, where the (-) sign is attributed to the clockwise contour enclosing the pole. For the pole $\alpha_p = \phi \pm \phi' + 2mn\pi$, the residue contribution is

$$U^c_{GO} = \mp U_0 \frac{\Psi(\pm\phi' + 2mn\pi + \frac{n\pi}{2})}{\Psi(\frac{n\pi}{2} - \phi')} e^{jk\rho\cos(\phi \pm \phi' + 2mn\pi)} \qquad (14)$$

By comparison with Table I, it is clear that the phase factor matches the geometrical phase term. However, it remains to show that the ratio of auxiliary Maliuzhinets functions is a product of reflection coefficients as in the geometrical analysis. For the incident GO field, which corresponds to $\beta=\beta^-=\phi-\phi'$, m=0, the ratio is obviously unity and no further consideration is necessary.

The ratio of auxiliary Maliuzhinets functions (and the leading sign) is denoted by $\Gamma_{\Pi}(\phi',\theta_0,\theta_n)$ and can be expanded in terms of Maliuzhinets functions using (6).

For $\beta = \beta^- = \phi-\phi'$

$$\Gamma_{\Pi}(\phi',\theta_0,\theta_n) = \frac{\Psi_n(-\phi' + n\pi + \frac{\pi}{2} - \theta_0 + 2mn\pi)}{\Psi_n(-\phi' + n\pi + \frac{\pi}{2} - \theta_0)} \qquad (15)$$

$$\cdot \frac{\Psi_n(-\phi' + n\pi - \frac{\pi}{2} + \theta_0 + 2mn\pi)}{\Psi_n(-\phi' + n\pi - \frac{\pi}{2} + \theta_0)}$$

$$\cdot \frac{\Psi_n(-\phi' + \frac{\pi}{2} - \theta_n - 2mn\pi)}{\Psi_n(-\phi' + \frac{\pi}{2} - \theta_n)}$$

$$\cdot \frac{\Psi_n(-\phi' - \frac{\pi}{2} + \theta_n + 2mn\pi)}{\Psi_n(-\phi' - \frac{\pi}{2} + \theta_n)}$$

and for $\beta = \beta^+ = \phi+\phi'$

$$\Gamma_{\Pi}(\phi',\theta_0,\theta_n) = \frac{\Psi_n(\phi' + n\pi + \frac{\pi}{2} - \theta_0 + 2mn\pi)}{\Psi_n(\phi' - n\pi + \frac{\pi}{2} - \theta_0)} \tag{16}$$

$$\cdot \frac{\Psi_n(\phi' + n\pi - \frac{\pi}{2} + \theta_0 + 2mn\pi)}{\Psi_n(\phi' - n\pi - \frac{\pi}{2} + \theta_0)}$$

$$\cdot \frac{\Psi_n(\phi' + \frac{\pi}{2} - \theta_n + 2mn\pi)}{\Psi_n(\phi' + \frac{\pi}{2} - \theta_n)}$$

$$\cdot \frac{\Psi_n(\phi' - \frac{\pi}{2} + \theta_n + 2mn\pi)}{\Psi_n(\phi' - \frac{\pi}{2} + \theta_n)}$$

The two single reflections are considered first since both are exceptional cases. Each can be reduced to a single reflection coefficient using the trigonometric identity

$$\tan \tfrac{1}{2}(\varphi-\theta) \cot \tfrac{1}{2}(\varphi-\theta) = \frac{\sin\varphi - \sin\theta}{\sin\varphi + \sin\theta} \tag{17}$$

For the reflection from face 0 ($\beta=\beta^+$, $m=0$) the last two terms in (15) and (16) reduce to unity. Using (6), the ratio $\Gamma_{\Pi}(\phi',\theta_0,\theta_n) = \Gamma_0(\phi')$. Similarly for the single reflection term from face n ($\beta=\beta^+$, $m= -1$) the first two terms of (15) and (16) reduce to unity. Using (6), the ratio $\Gamma_{\Pi}(\phi',\theta_0,\theta_n) = \Gamma_n(n\pi - \phi')$.

The higher order reflection coefficients remain to be considered. To obtain the appropriate products of reflection coefficients for the higher order reflections, the required identities are

$$\frac{\Psi_n(x + 2mn\pi)}{\Psi_n(x)} = \prod_{\ell=1}^{m} \frac{\Psi_n(x + (2\ell-1)n\pi + n\pi)}{\Psi_n(x + (2\ell-1)n\pi - n\pi)} \qquad m > 0 \tag{18}$$

$$\frac{\Psi_n(x + 2mn\pi)}{\Psi_n(x)} = \prod_{\ell=1}^{|m|} \frac{\Psi\ (x + (1-2\ell)n\pi - n\pi)}{\Psi_n(x + (1-2\ell)n\pi + n\pi)} \qquad m < 0 \qquad (19)$$

These are just algebraic identities, true for any function, which are easily verified by expanding the product.

Using (6)-(8) and (15)-(19), the geometrical optics residues can be reduced completely to products of reflection coefficients. The final forms of the geometrical optics residues are

<u>For $\beta = \beta^- = \phi - \phi'$, $m>0$</u>

$$\Gamma_{\Pi}(\phi', \theta_0, \theta_n) = \prod_{\ell=1}^{m} \Gamma_0(2\ell n\pi - \phi') \prod_{\ell=1}^{m} \Gamma_n((2\ell-1)n\pi - \phi') \qquad (20)$$

<u>For $\beta = \beta^- = \phi - \phi'$, $m<0$</u>

$$\Gamma_{\Pi}(\phi', \theta_0, \theta_n) = \prod_{\ell=1}^{|m|} \Gamma_0(\phi' + (2\ell-2)n\pi) \prod_{\ell=1}^{|m|} \Gamma_n(\phi' + (2\ell-1)n\pi) \qquad (21)$$

<u>For $\beta = \beta^+ = \phi + \phi'$, $m>0$</u>

$$\Gamma_{\Pi}(\phi', \theta_0, \theta_n) = \prod_{\ell=1}^{m+1} \Gamma_0(\phi' + (2\ell-2)n\pi) \prod_{\ell=1}^{m} \Gamma_n(\phi' + (2\ell-1)n\pi) \qquad (22)$$

<u>For $\beta = \beta^+ = \phi + \phi'$, $m<-1$</u>

$$\Gamma_{\Pi}(\phi', \theta_0, \theta_n) = \prod_{\ell=1}^{|m+1|} \Gamma_0(2\ell n\pi - \phi') \prod_{\ell=1}^{|m|} \Gamma_n(2(\ell-1)n\pi - \phi') \qquad (23)$$

The cases $(\beta^-, m=0)$, $(\beta^+, m=0)$, $(\beta^+, m=-1)$ are the incident and singly reflected terms already considered. By comparison with Table I, it is evident that these expressions are identical to the geometrical ray tracing analysis.

IV. THE UNIFORM DIFFRACTED FIELD

The diffracted field contribution is obtained from an asymptotic evaluation of the integral contribution along the steepest descent paths. The approximation of the integral uniformly accounts for the effects of poles passing through the saddle points. The modified Pauli-Clemmow method of steepest descents is utilized to assure that the diffracted field provides the proper continuity across geometrical optics shadow boundaries as the geometrical optics poles pass into or out of the region between the steepest descent paths. As in the uniform geometrical theory of diffraction for the perfect conductor case, the effect of the four poles nearest the steepest descent paths will be considered, thereby yielding four Fresnel transition functions. The major difference for the impedance wedge problem is the multiplying factor preceding each cotangent-Fresnel term. These multiplying factors are the auxiliary Maliuzhinets function ratios which provide the proper continuity in the reflected field. The discontinuities in the diffracted field are precisely equal and opposite to the discontinuities of the geometrical optics field at the shadow boundaries.

The diffracted field is written as

$$U_D = U_0 \frac{e^{-jk\rho}}{\sqrt{\rho}} \left[- \frac{e^{-j\pi/4}}{2n\sqrt{2\pi k}} \right] \cdot \tag{24}$$

$$\left[\frac{\Psi(-\pi + \frac{n\pi}{2} - \phi)}{\Psi(\frac{n\pi}{2} - \phi')} \cot(\frac{\pi + \beta^-}{2n}) F\left[k\rho(1 + \cos(\beta^- - 2n\pi N_-^+))\right] \right.$$

$$\left. + \frac{\Psi(\pi + \frac{n\pi}{2} - \phi)}{\Psi(\frac{n\pi}{2} - \phi')} \cot(\frac{\pi - \beta^-}{2n}) F\left[k\rho(1 + \cos(\beta^- - 2n\pi N_-^-))\right] \right]$$

$$- \frac{\Psi(-\pi + \frac{n\pi}{2} - \phi)}{\Psi(\frac{n\pi}{2} - \phi')} \cot(\frac{\pi + \beta^+}{2n}) F\left[k\rho(1 + \cos(\beta^+ - 2n\pi N_+^+))\right]$$

$$- \frac{\Psi(\pi + \frac{n\pi}{2} - \phi)}{\Psi(\frac{n\pi}{2} - \phi')} \cot(\frac{\pi - \beta^+}{2n}) F\left[k\rho(1 + \cos(\beta^+ - 2n\pi N_+^-))\right]\Bigg]$$

where F[x] is the Fresnel transition function of [8] and where the N's are integers which most nearly satisfy

$$2\pi n N_-^+ - \beta^- = +\pi \tag{25a}$$

$$2\pi n N_-^- - \beta^- = -\pi \tag{25b}$$

$$2\pi n N_+^+ - \beta^+ = +\pi \tag{25c}$$

$$2\pi n N_+^- - \beta^+ = -\pi \tag{25d}$$

Near the shadow boundaries, the cotangent function becomes very large while the Fresnel transition function approaches zero. Together they provide the proper discontinuity at the shadow boundary. However the cotangent-Fresnel product is not a computationally effective formulation for determining this discontinuity accurately. A better formulation is to use the first term of the cotangent Laurent series and the first two terms of the small argument form of the Fresnel transition function. The result is to use the approximation

$$\cot(\frac{\pi \pm \beta}{2n}) F\left[k\rho(1 + \cos(\beta - 2n\pi N)\right] \tag{26}$$

$$\simeq n\left[\sqrt{2\pi k\rho}\ \mathrm{sgn}\ \varepsilon - 2k\rho\ \varepsilon\ e^{j\pi/4}\right] e^{j\pi/4}$$

where ε is small and, depending on which cotangent-Fresnel product is replaced, ε is given by one of the following expressions.

$$\varepsilon = \pi + \beta^- - 2n\pi N_-^+ \tag{27a}$$

$$\varepsilon = \pi - \beta^- + 2n\pi\, N_-^- \tag{27b}$$

$$\varepsilon = \pi + \beta^+ - 2n\pi\, N_+^+ \tag{27c}$$

or $$\varepsilon = \pi - \beta^+ + 2n\pi\, N_+^- \tag{27d}$$

V. THE SURFACE WAVE

The surface wave is a wave which propagates along one face of the wedge and which is typically exponentially decaying away from the face. It is confined to a particular angular range from the wedge face whenever it exists. Since the wave may decay slowly along the face, its contribution can be more dominant than other scattering mechanisms near the wedge surface.

The surface wave is determined by the residues of enclosed poles of the Maliuzhinets function between the steepest descent paths. The surface wave poles are located at [1], [5],

$$\alpha_0 = \phi + \pi + \theta_0 \tag{28a}$$

$$\alpha_n = \phi - n\pi - \pi - \theta_n \tag{28b}$$

for the 0 and n faces, respectively. As for the geometrical optics poles, the α_0 pole moves from $\pi + \theta_0$ to $n\pi + \pi + \theta_0$ as ϕ increases from 0 to $n\pi$ while the α_n pole moves from $-n\pi - \pi - \theta_n$ to $-\pi - \theta_n$. These loci are shown in Fig. 2. The α_0 pole can only be within the steepest descent paths for ϕ less than some maximum value. Similarly, the α_n pole can only be within the steepest descent paths for ϕ greater than some minimum value. Hence each surface wave term is bounded to a region

near the corresponding face. In general the surface waves corresponding to the pole α exists if

$$-\pi < \alpha_r - \cos^{-1}(1/\cosh(\alpha_i))\ \mathrm{sgn}\ \alpha_i < \pi \tag{29}$$

where $\alpha = \alpha_r + j\alpha_i$.

To determine the pole residue, (9) is used. This expression isolates the singular part of the pole in the cosecant function and hence the residue is readily calculated. The surface waves are

$$U_{sw}^{0} = U_0 \frac{2\sin\frac{\pi}{2n}}{\psi(\frac{n\pi}{2} - \phi')} \frac{\sin\frac{\phi'}{n}}{\cos(\frac{\pi+\theta_0}{n}) - \cos(\frac{\phi'}{n})} e^{-jk\rho\cos(\phi+\theta_0)} \tag{30a}$$

$$\cdot\ \psi_n(n\pi - \tfrac{\pi}{2})\ \psi_n(\tfrac{\pi}{2} + n\pi + 2\theta_0)\ \psi_n(\tfrac{3\pi}{2} + \theta_0 - \theta_n)\ \psi_n(\tfrac{\pi}{2} + \theta_0 + \theta_n)$$

$$U_{sw}^{n} = U_0 \frac{-2\sin\frac{\pi}{2n}}{\psi(\frac{n\pi}{2} - \phi')} \frac{\sin\frac{\phi'}{n}}{\cos(\frac{n\pi+\pi+\theta_0}{n}) - \cos(\frac{\phi'}{n})} e^{-jk\rho\cos(\phi-n\pi-\theta_n)} \tag{30b}$$

$$\cdot\ \psi_n(n\pi - \tfrac{\pi}{2})\ \psi_n(\tfrac{\pi}{2} + n\pi + 2\theta_n)\ \psi_n(\tfrac{3\pi}{2} + \theta_n - \theta_0)\ \psi_n(\tfrac{\pi}{2} + \theta_0 + \theta_n)$$

By the symmetry of the wedge, it is noted that either of these can be obtained from the other by the replacement of ϕ by $n\pi-\phi$, ϕ' by $n\pi-\phi'$, θ_0 by θ_n, and θ_n by θ_0.

As a surface wave pole moves outside the steepest descent paths, the contribution of the surface wave term vanishes. Hence a discontinuity exists at the boundary of the surface wave region. In addition the contribution of the steepest descent path integration is affected by the nearby surface wave pole. The integral can be uniformly evaluated to account for the nearby pole using the steepest descent method of Felsen and Marcuvitz [10]. This formulation provides

the proper continuity in the total field as the surface wave pole crosses the steepest descent path. The asymptotic evaluation of the integral introduces a Fresnel transition function of complex argument. The surface wave transition field is

$$U^0_{SWTR} = U_0 \frac{e^{-jk\rho}}{\sqrt{\rho}} \frac{-\sqrt{j}}{\pi} \sin\frac{\pi}{2n} \frac{\sin\frac{\phi'}{n}}{\Psi(\frac{n\pi}{2} - \phi')} \frac{}{\cos(\frac{\pi+\theta_0}{n}) - \cos(\frac{\phi'}{n})} \tag{31a}$$

$$\cdot \Psi_n(n\pi - \tfrac{\pi}{2}) \Psi_n(n\pi + \tfrac{\pi}{2} + 2\theta_0) \Psi_n(\tfrac{3\pi}{2} + \theta_0 - \theta_n) \Psi_n(\tfrac{\pi}{2} + \theta_0 + \theta_n)$$

$$\cdot \frac{\left[F[k\rho(1 - \cos(\phi+\theta_0))] - 1\right]}{\sqrt{k\rho(\cos(\phi+\theta_0) - 1)}}$$

$$U^n_{SWTR} = U_0 \frac{e^{-jk\rho}}{\sqrt{\rho}} \frac{\sqrt{j}}{\pi} \sin\frac{\pi}{2n} \frac{\sin\frac{\phi'}{n}}{\Psi(\frac{n\pi}{2} - \phi')} \frac{}{\cos(\frac{n\pi+\pi+\theta_n}{n}) - \cos(\frac{\phi'}{n})} \tag{31b}$$

$$\cdot \Psi_n(n\pi - \tfrac{\pi}{2}) \Psi_n(n\pi + \tfrac{\pi}{2} + 2\theta_0) \Psi_n(\tfrac{3\pi}{2} + \theta_n - \theta_0) \Psi_n(\tfrac{\pi}{2} + \theta_0 + \theta_n)$$

$$\cdot \frac{\left[F[k\rho(1 - \cos(\phi-n\pi-\theta_n))] - 1\right]}{\sqrt{k\rho(1-\cos(\phi-n\pi-\theta_n))}}$$

This Fresnel transition function is as defined in [8] but extended to complex argument. The $\sqrt{z}$ in the definition of F[z] should have a branch cut along the positive imaginary axis so that $-\frac{3\pi}{4} < \arg\sqrt{z} < \frac{\pi}{4}$. When the pole is far from the steepest descent path, the Fresnel transition function is approximately unity, and hence the surface wave transition field contribution is zero.

A troublesome case occurs when the surface wave pole coincides with a geometrical optics pole. Since geometrical optics poles are

always real, this can only occur for real surface impedances. Real surface impedances, however, cannot support surface waves as the surface wave pole will never lie within the steepest descent paths. However if the surface wave transition field is calculated by blindly applying (31a) and (31b), erroneously large results will occur whenever the surface wave pole is far from the steepest descent paths yet near a geometrical optics pole. Indeed the surface wave transition field should be zero when the surface wave pole is far from the steepest descent paths. Hence expressions (31a) and (31b) should only be used when the surface wave pole is closer to a steepest descent path than it is to a geometrical optics pole. When the surface wave pole is far from the steepest descent path, the surface wave transition field should be taken as zero.

VI. NUMERICAL RESULTS

Using the uniform diffraction theory developed in this paper, diffraction patterns of various wedge configurations were computed. The wedges studied in this section are all interior wedges although the theory is equally useful for exterior wedges. The formulation can be used to study the field in the vicinity of the wedge when the wedge is illuminated by a plane wave, and by reciprocity, it can also be used to examine the far field pattern of a line source located within the interior impedance wedge.

For the plane wave diffraction problem, the plane wave is incident from the direction $\phi'=30^\circ$ measured from the 0 face of the wedge. The

field pattern is determined at a distance $\rho=1.6\lambda$ from the edge of the wedge at an angle ϕ. The total field is normalized to an incident plane wave of unity. For the line source diffraction problem, the line source is located at a distance $\rho=1.6\lambda$ from the edge of the wedge at an angle $\phi'=30^{\circ}$ from the 0 face. The far field pattern is determined in the direction ϕ and the total field is normalized to a line source field of unity. Both hard and soft polarizations are considered for surface impedances which may be real or complex. For any of the illustrated patterns, the opposite polarization is implicitly given by the same figure using the reciprocal of the normalized surface impedance shown.

In Figs. 3 and 4, the effect of increasing the surface loss in the wedge faces is examined for the far field pattern of a line source within the interior wedge. Fig. 3 shows the soft polarization while Fig. 4 gives the hard polarization results. The wedge has an interior angle of 98° and has a normalized surface impedance of 0.0, 0.25, or 0.50. The case $\eta=0.0$ corresponds to the perfectly conducting wedge and for this case the soft polarized field of Fig. 3 is zero on the face of the wedge. For the hard polarized field of Fig. 4, the field is nonzero on the face of the wedge when the surface is perfectly conducting. As the loss increases to $\eta=0.25$ and then to $\eta=0.50$, the reflected and diffracted fields rapidly diminish. The total field approaches the normalized value of unity corresponding to the incident field of the line source alone as the surface loss increases.

In Fig. 5, the effect of the reactive portion of the complex surface impedance is examined. The line source diffraction problem is considered, and the far field pattern is computed. An interior wedge

angle of 98° is chosen and the soft polarized case is shown. The normalized surface impedance values range from 0.5-j1.0 to 0.5+j1.0. The reactive portion of the surface impedance effectively causes a phase change of the reflection and diffraction coefficients. Since the structure of the lobes of the far field pattern is determined by the relative phases of the various scattering components, the far field pattern is very sensitive to changes in the reactive portion of the surface impedance.

In Figs. 6 and 7, the field patterns for various wedge angles are shown. The interior wedge angles are 90°, 98° and 77° and a normalized complex surface impedance of η=0.5-j1.0 was selected. In Fig. 6 the far field pattern of a line source within the wedge structure is shown. In Fig. 7, the field pattern in the vicinity of the wedge is given for plane wave incidence from the direction ϕ'=30°. It is evident that the field pattern is greatly changed by increasing or decreasing the interior wedge angle. This is markedly different than the exterior wedge case for which the field pattern is quite insensitive to the exterior wedge angle except for in the vicinity of the wedge face. A notable difference between the line source far field pattern problem and the incident plane wave diffraction problem is observed at the wedge faces. For the line source within the lossy impedance wedge, the geometrical optics field always goes to zero at the wedge faces because the reflected field approaches grazing incidence. At grazing incidence the reflection coefficient becomes -1 for both polarizations, and the reflected field cancels the incident field. This is not the case for the incident plane wave diffraction problem because the incident field

does not approach at grazing incidence when the field observation point is located near a wedge face. In general, the geometrical optics field will not be zero on the faces of the lossy impedance wedge for an incident plane wave.

In Figs. 8 and 9, the individual scattering mechanisms are illustrated for the soft polarization plane wave incidence case with normalized surface impedances of $0.1+j0.2$. In Fig. 8, a 90° interior wedge is considered. For the right angled wedge, the solution can be analyzed entirely using image theory; hence only the incident and geometrical optics terms appear and all other terms are zero. In Fig. 9, an 85° interior wedge is considered and for this wedge angle the image theory is not sufficient. Discontinuities in the reflected field occur at $\phi=20^\circ$ and $\phi=40^\circ$ corresponding to shadow boundaries of the double reflected fields $\underline{0n}$ and $\underline{n0}$, respectively. The discontinuities in the diffracted field exactly compensate for the geometrical optics discontinuities. In addition, a surface wave exists on each face and the surface wave boundaries appear at approximately $\phi=6^\circ$ and $\phi=79^\circ$. The surface wave transition field exactly compensates for the surface wave discontinuities and the resultant total field is continuous everywhere.

VII. CONCLUSION

A uniform asymptotic evaluation of the exact integral solution for the field scattered by interior impedance wedges has been performed. The case of normal incidence on a wedge with uniform but different

impedances on each face was considered for both soft (E_z) and hard (H_z) polarizations. The results are applicable to both the interior and exterior wedges although the interior case is emphasized in the numerical results presented. The uniform asymptotic evaluation separates the individual components of the total field. The extracted terms include the incident and singly reflected fields, the multiply reflected fields, the edge diffracted field, the surface waves and the surface wave transition fields.

The singly and multiply reflected fields, written as ratios of Maliuzhinets functions, were shown to be identical to the product of reflection coefficients and phase factors obtained from a geometrical ray tracing analysis. The reflection coefficients used are appropriate for plane wave incidence on an infinite planar uniform impedance surface. The pole positions between the steepest descent paths determined the angular range over which the multiply reflected fields exist, and these limits matched those determined using the ray tracing approach.

The diffracted field is calculated from the modified Pauli-Clemmow method of steepest descents. The four poles nearest the steepest descent paths are considered and hence four Fresnel transition functions are obtained. The diffracted field provides the proper discontinuity to compensate for the discontinuity in the incident, singly reflected, and multiply reflected fields. The formulation is analogous to the perfect conductor case with the introduction of ratios of auxiliary Maliuzhinets functions as multiplicative factors. These factors are necessary because the reflection coefficients are not ± 1 as

in the perfect conductor case. The cotangent-Fresnel functions are computationally difficult to evaluate near shadow boundaries, and alternate expressions are presented for use near the boundaries. These small-argument expressions are more computationally effective for accurate calculation of the discontinuity.

The surface wave and the associated surface wave transition field were presented, and the range of existence of each surface wave was identified. The surface wave exists over a finite angular range for a particular surface impedance, and the surface wave transition field is added to provide the proper continuity across the surface wave boundaries. Even if the surface wave does not exist, the surface wave pole may be near the steepest descent path and hence the surface wave transition function should be included. For observations far from the surface wave boundaries, the surface wave transition function vanishes and only the geometrical optics, diffracted, and surface wave terms are important. The surface wave generally decays exponentially away from the associated surface, but it might be only weakly attenuated along the surface face. Hence the surface wave term could be the most dominant term near the surface, depending on the value of the surface impedance.

VIII. PUBLICATIONS

During this reporting period three refereed papers supported by this NASA Grant have appeared in IEEE publications. These papers are the following:

1. T. Griesser and C. A. Balanis, "Backscatter analysis of dihedral corner reflectors using the phsyical theory of diffraction," *IEEE Trans. Antennas Propagat.*, vol. AP-35, no. 10, pp. 1137-1147, October 1987.

2. T. Griesser and C. A. Balanis, "Dihedral corner reflector backscatter using higher-order reflections and diffractions," *IEEE Trans. Antennas Propagat.*, vol. AP-35, no. 11, pp. 1235-1247, November 1987.

3. D. P. Marsland, C. A. Balanis and S. Brumley, "Higher-order diffractions from a circular disk," *IEEE Trans. Antennas Propagat.*, vol. AP-35, no. 12, December 1987.

IX. FUTURE WORK

Future work on this project will concentrate on applying these interior wedge diffraction function to predict the scattering patterns of corner reflectors with finite size plates. The contributions of surface waves will also be accounted for.

REFERENCES

[1] G. D. Maliuzhinets, "Excitation, reflection and emission of surface waves from a wedge with given face impedances," Soviet Physics, Doklady, vol. 3, pp. 752-755, 1958.

[2] G. D. Malyughinetz (Maliuzhinets), "Das Sommerfeldsche Integral und die Losung von Beugungsaufgaben in Winkelgebieten," Annalen der Physik, Folge 7, Band 6, Heft 1-2, pp. 107-112, 1960.

[3] O. M. Bucci and G. Franceschetti, "Electromagnetic scattering by a half plane with two face impedances," Radio Science, vol. 11, no. 1, pp. 49-59, Jan. 1976.

[4] R. Tiberio, G. Pelosi, and G. Manara, "A uniform GTD formulation for the diffraction by a wedge with impedance faces," IEEE Trans. Ant. Prop., vol. AP-33, no. 8, pp. 867-873, Aug. 1985.

[5] M. I. Herman and J. L. Volakis, "High frequency scattering from canonical impedance structures," University of Michigan Radiation Laboratory, Report 389271-T, Ann Arbor, MI, pp. 88-101, May 1987.

[6] J. J. Bowman, "High-frequency backscattering from an absorbing infinite strip with arbitrary face impedances," Canadian J. Physics, vol. 45, pp. 2409-2430, 1967.

[7] T. B. A. Senior, "A note on impedance boundary conditions," Canadian J. Physics, vol. 40, pp. 663-665, May 1962.

[8] R. G. Kouyoumjian and P. H. Pathak, "A uniform geometrical theory of diffraction for an edge on a perfectly conducting surface," Proc. IEEE, vol. 62, no. 11, pp. 1448-1461, Nov. 1974.

[9] P. H. Pathak and R. G. Kouyoumjian, "The dyadic diffraction coefficient for a perfectly conducting wedge," Air Force Cambridge Research Laboratories, Technical Report 2183-4, Bedford, MA, June 5, 1970.

[10] L. B. Felsen and N. Marcuvitz, Radiation and Scattering of Waves, New Jersey: Prentice Hall, 1973, p. 399.

[11] P. C. Clemmow, The Plane Wave Spectrum Representation of Electromagnetic Fields, Oxford: Pergamon Press, 1966, pp. 43-58.

TABLE I

ASSOCIATION OF THE GEOMETRICAL OPTICS TERMS WITH THE POLE RESIDUES

Comp	Pole	$\Gamma_{\Pi}(\phi', \theta_0, \theta_n)$	α_p	Existence
0n0n	β^-, m=-2	$\Gamma_0(\phi')\Gamma_n(n\pi+\phi')\Gamma_0(2n\pi+\phi')\Gamma_n(3n\pi+\phi')$	$\phi-\phi'-4n\pi$	$\phi-\phi'>4n\pi-\pi$
n0n	β^+, m=-2	$\Gamma_n(n\pi-\phi')\Gamma_0(2n\pi-\phi')\Gamma_n(3n\pi-\phi')$	$\phi+\phi'-4n\pi$	$\phi+\phi'>4n\pi-\pi$
0n	β^-, m=-1	$\Gamma_0(\phi')\Gamma_n(n\pi+\phi')$	$\phi-\phi'-2n\pi$	$\phi-\phi'>2n\pi-\pi$
n	β^+, m=-1	$\Gamma_n(n\pi-\phi')$	$\phi+\phi'-2n\pi$	$\phi+\phi'>2n\pi-\pi$
Inc	β^-, m=0	1	$\phi-\phi'$	$-\pi<\phi-\phi'<\pi$
0	β^+, m=0	$\Gamma_0(\phi')$	$\phi+\phi'$	$\phi+\phi'<\pi$
n0	β^-, m=1	$\Gamma_n(n\pi-\phi')\Gamma_0(2n\pi+\phi')$	$\phi-\phi'+2n\pi$	$\phi-\phi'<\pi-2n\pi$
0n0	β^+, m=1	$\Gamma_0(\phi')\Gamma_n(n\pi+\phi')\Gamma_0(2n\pi+\phi')$	$\phi+\phi'+2n\pi$	$\phi+\phi'<\pi-2n\pi$
n0n0	β^-, m=2	$\Gamma_n(n\pi-\phi')\Gamma_0(2n\pi-\phi')\Gamma_n(3n\pi-\phi')\Gamma_0(4n\pi-\phi')$	$\phi-\phi'+4n\pi$	$\phi-\phi'<\pi-4n\pi$

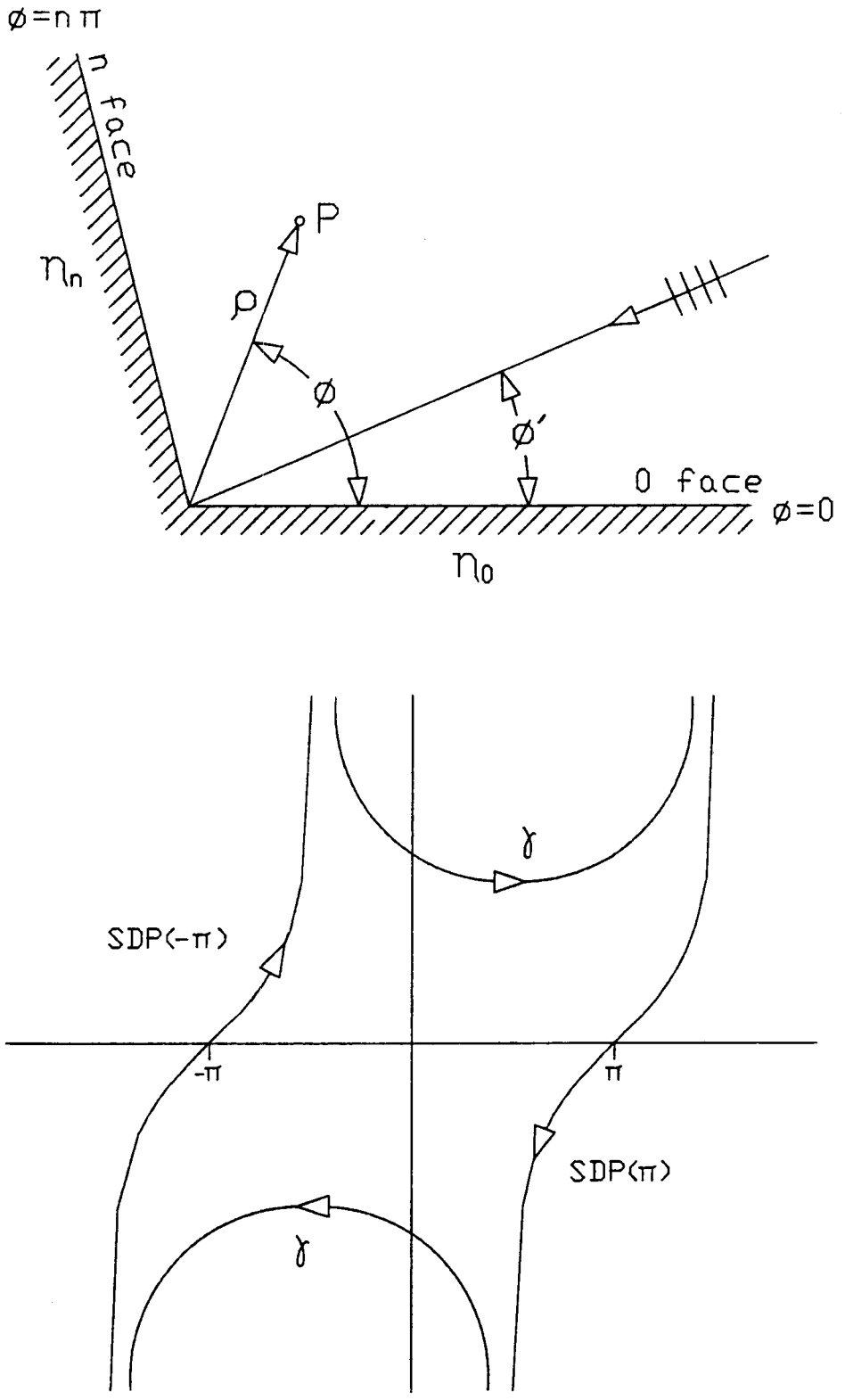

Fig. 1. Interior wedge geometry and integration contours for the exact impedance wedge solution.

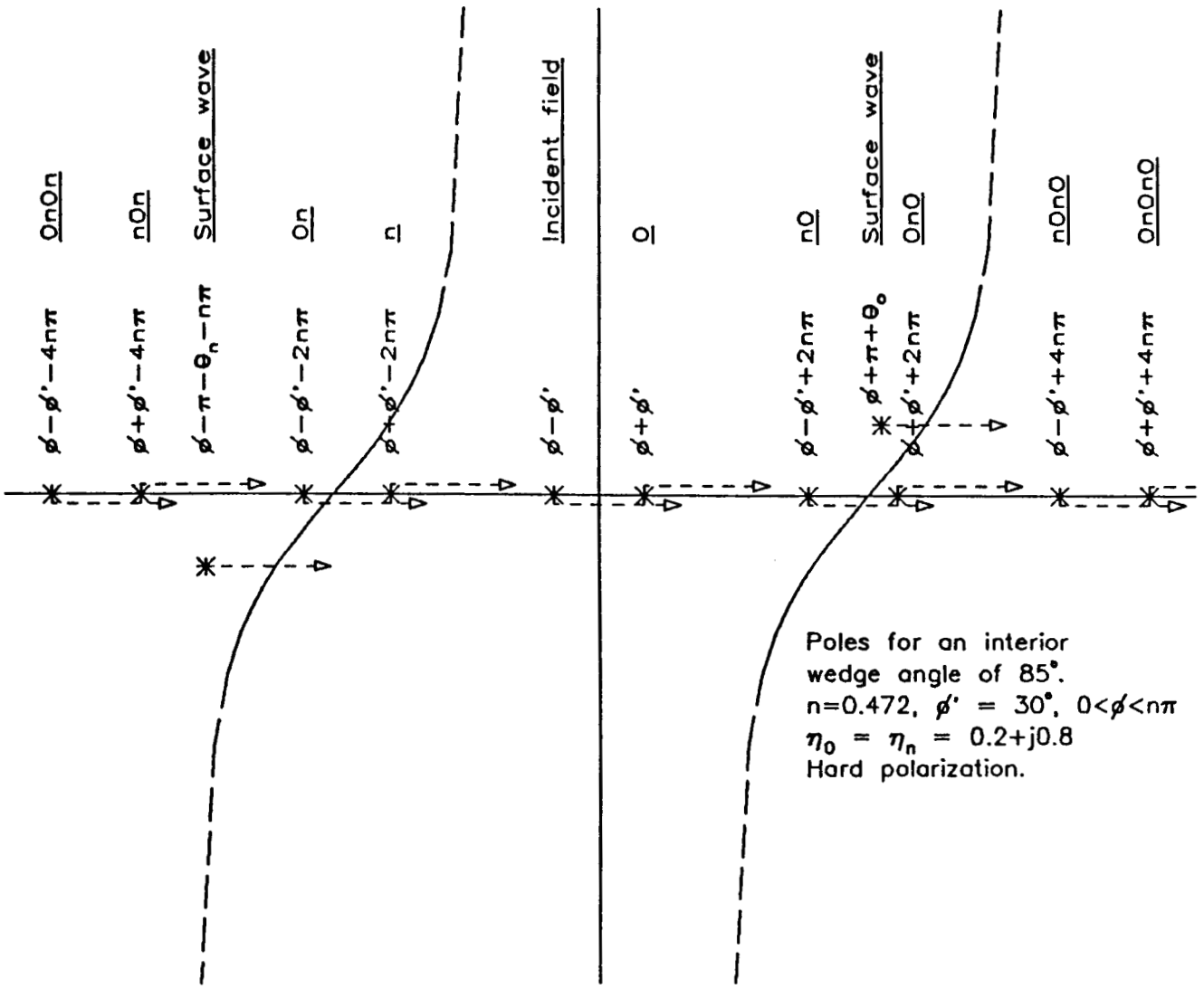

Fig. 2. Geometrical optics and surface wave poles in the complex plane corresponding to specific scattering terms.

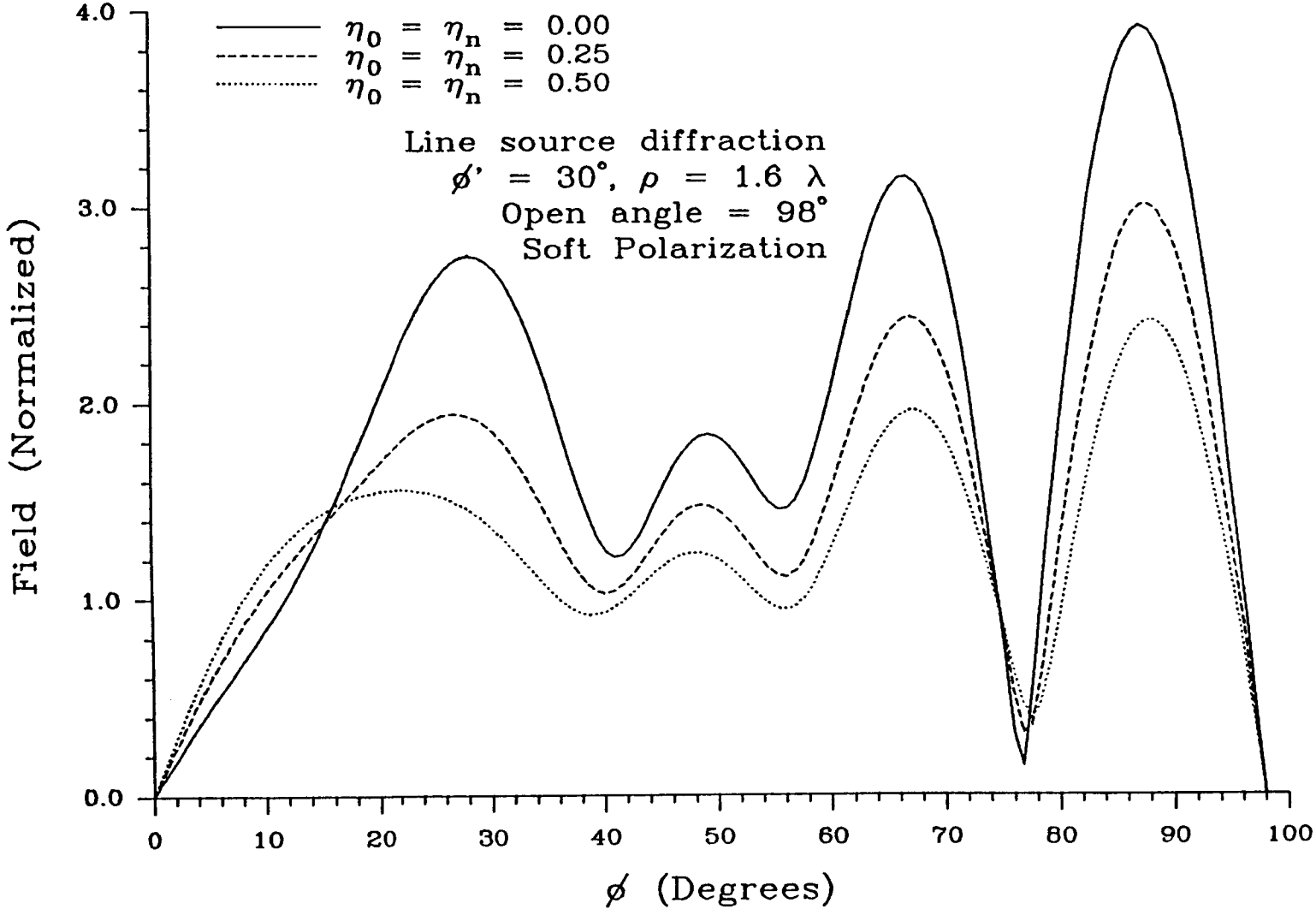

Fig. 3. Comparison of line source patterns for increasing surface impedances for the soft polarization case.

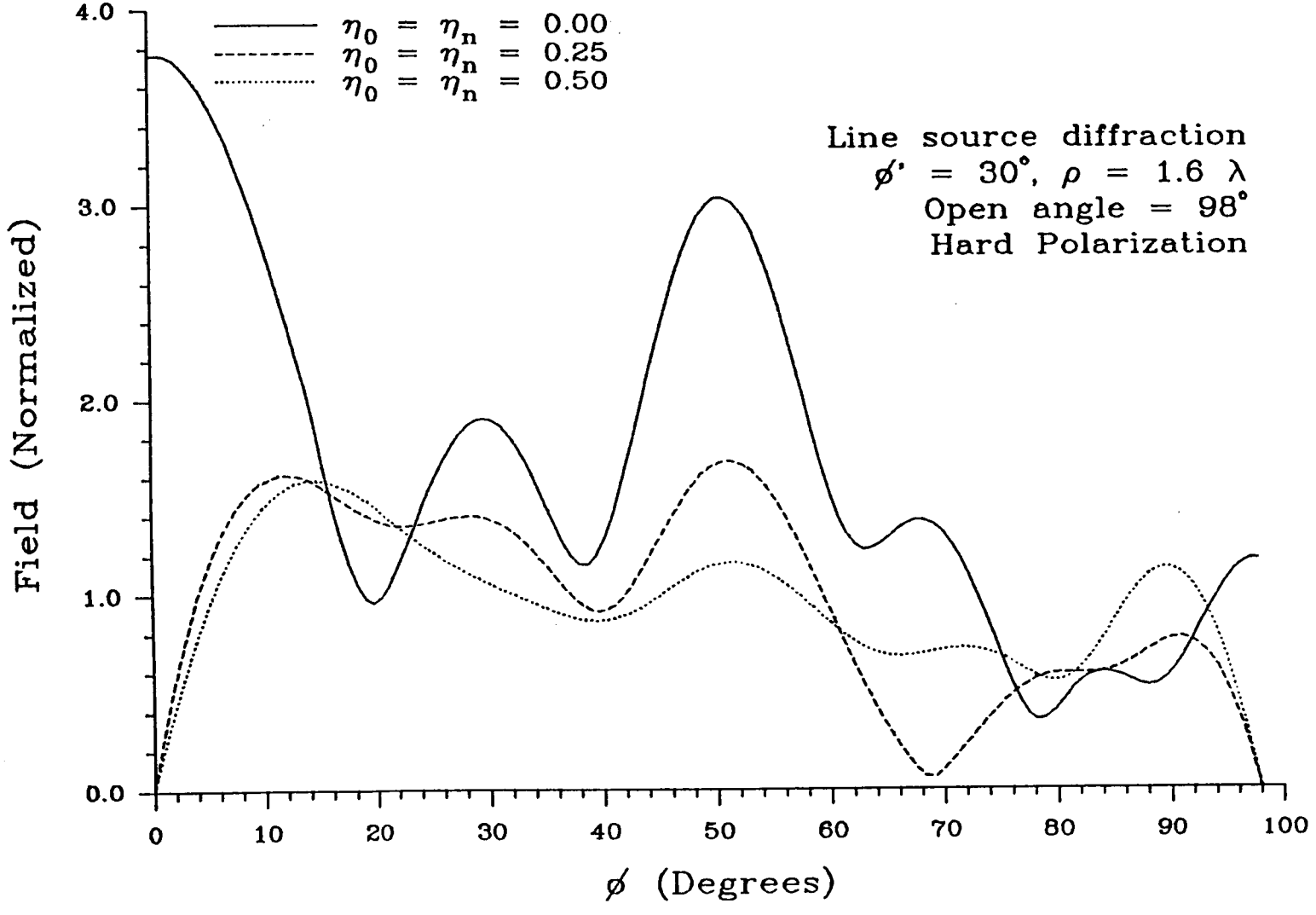

Fig. 4. Comparison of line source patterns for increasing surface impedances for the hard polarization case.

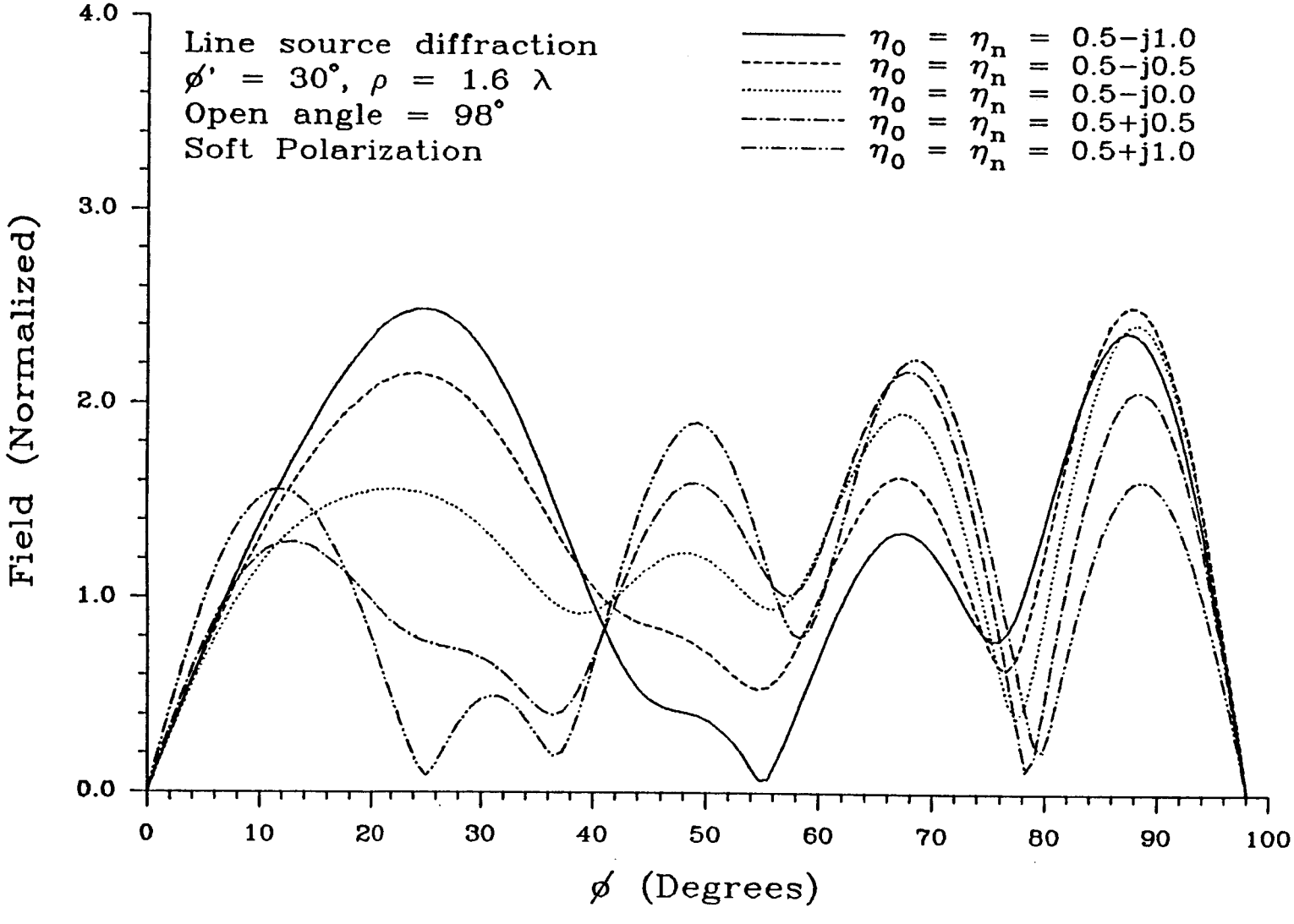

Fig. 5. Variation of the line source patterns for various complex surface impedances.

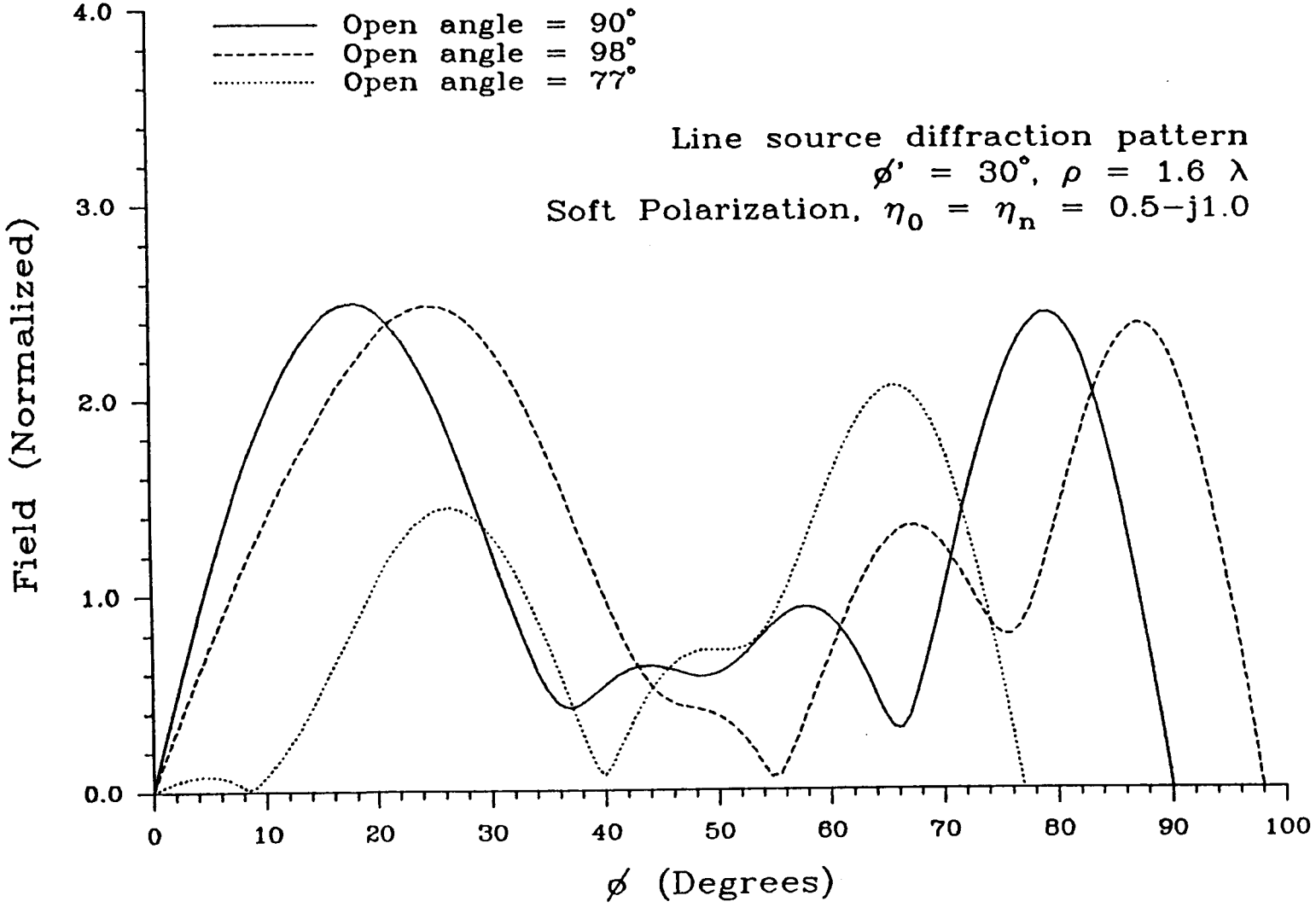

Fig. 6. Far field patterns of line sources within interior wedges of different angles.

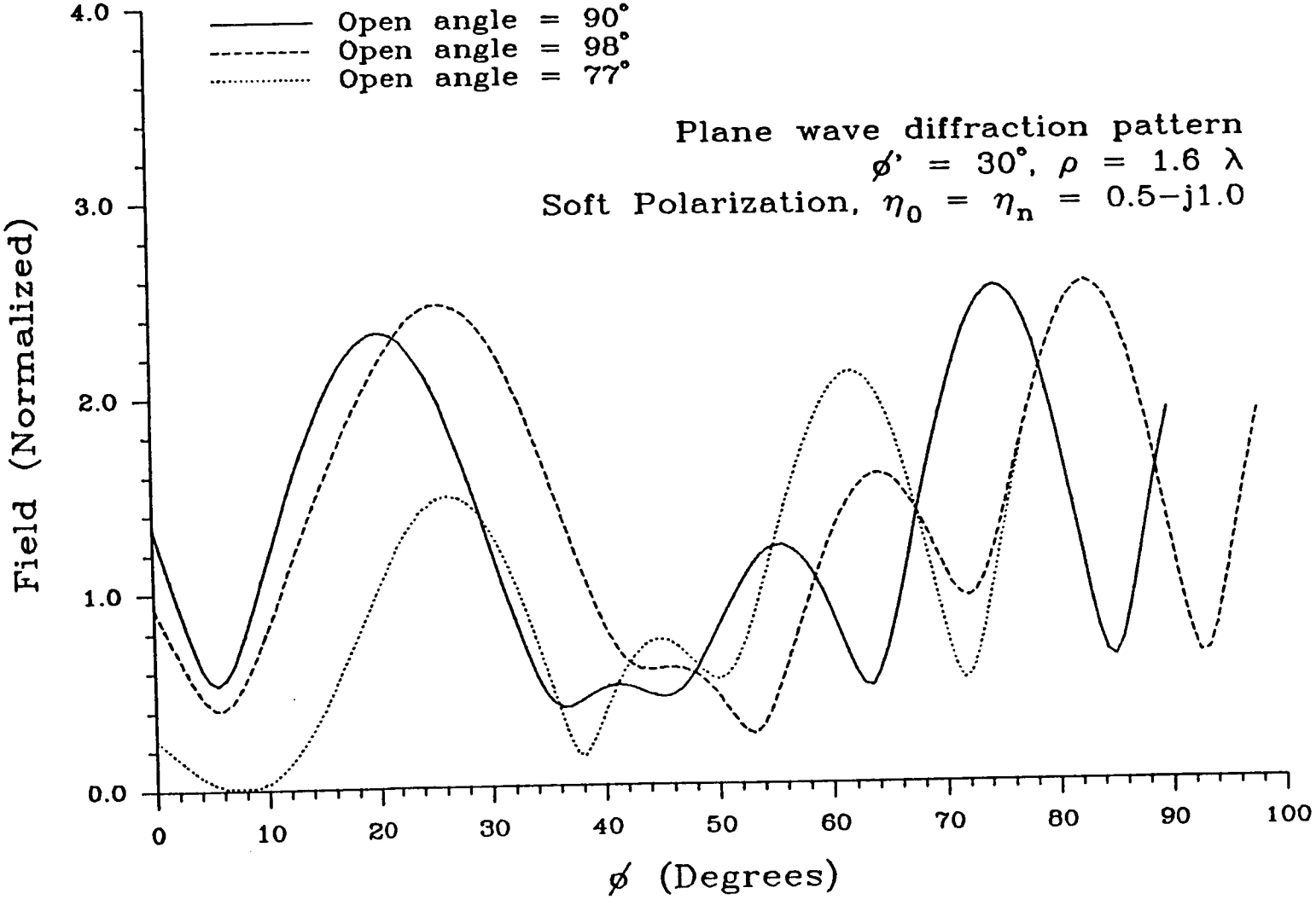

Fig. 7. Plane wave scattering patterns within interior wedges of different angles.

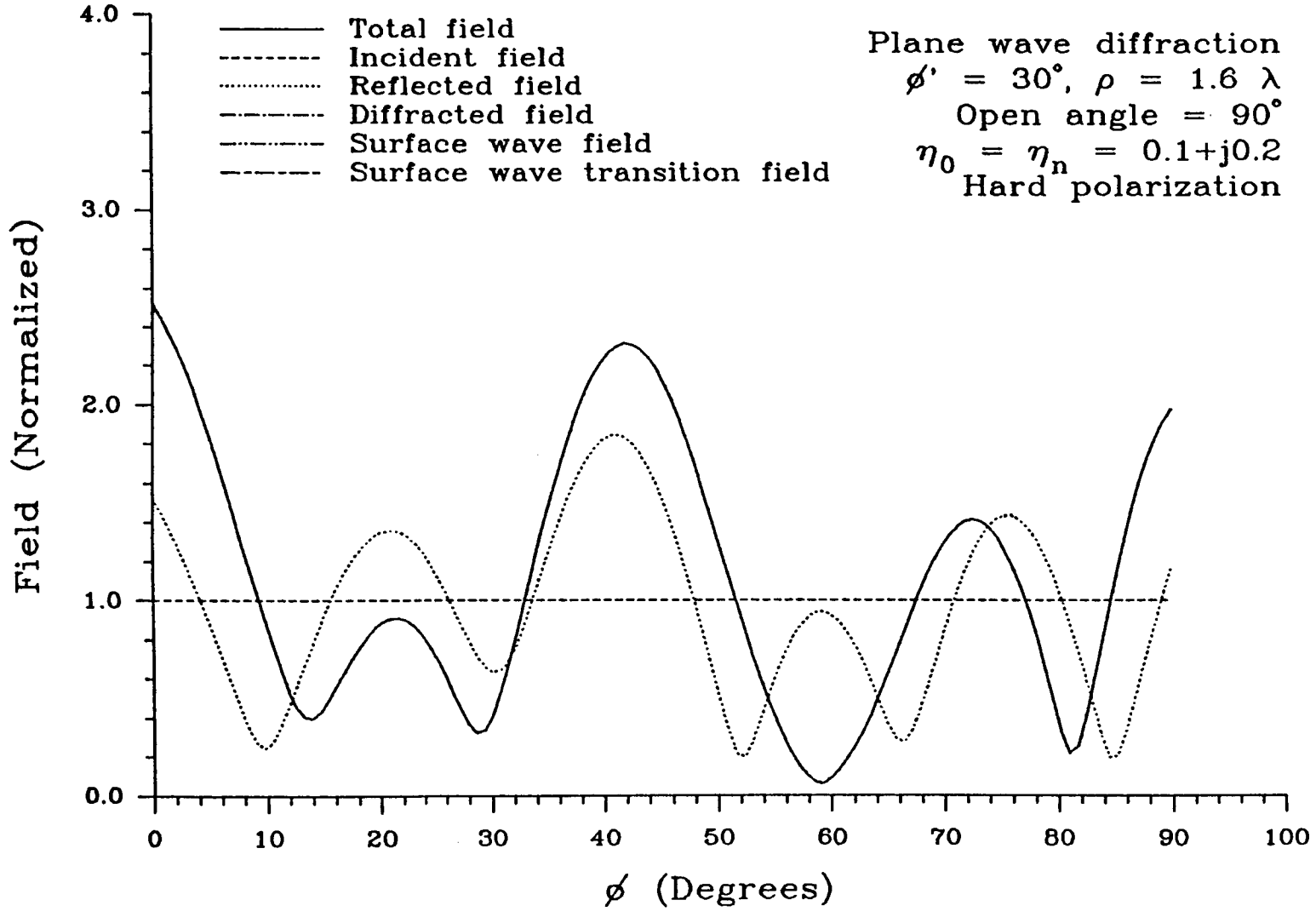

Fig. 8. Components of the total field of a right angled wedge for plane wave incidence.

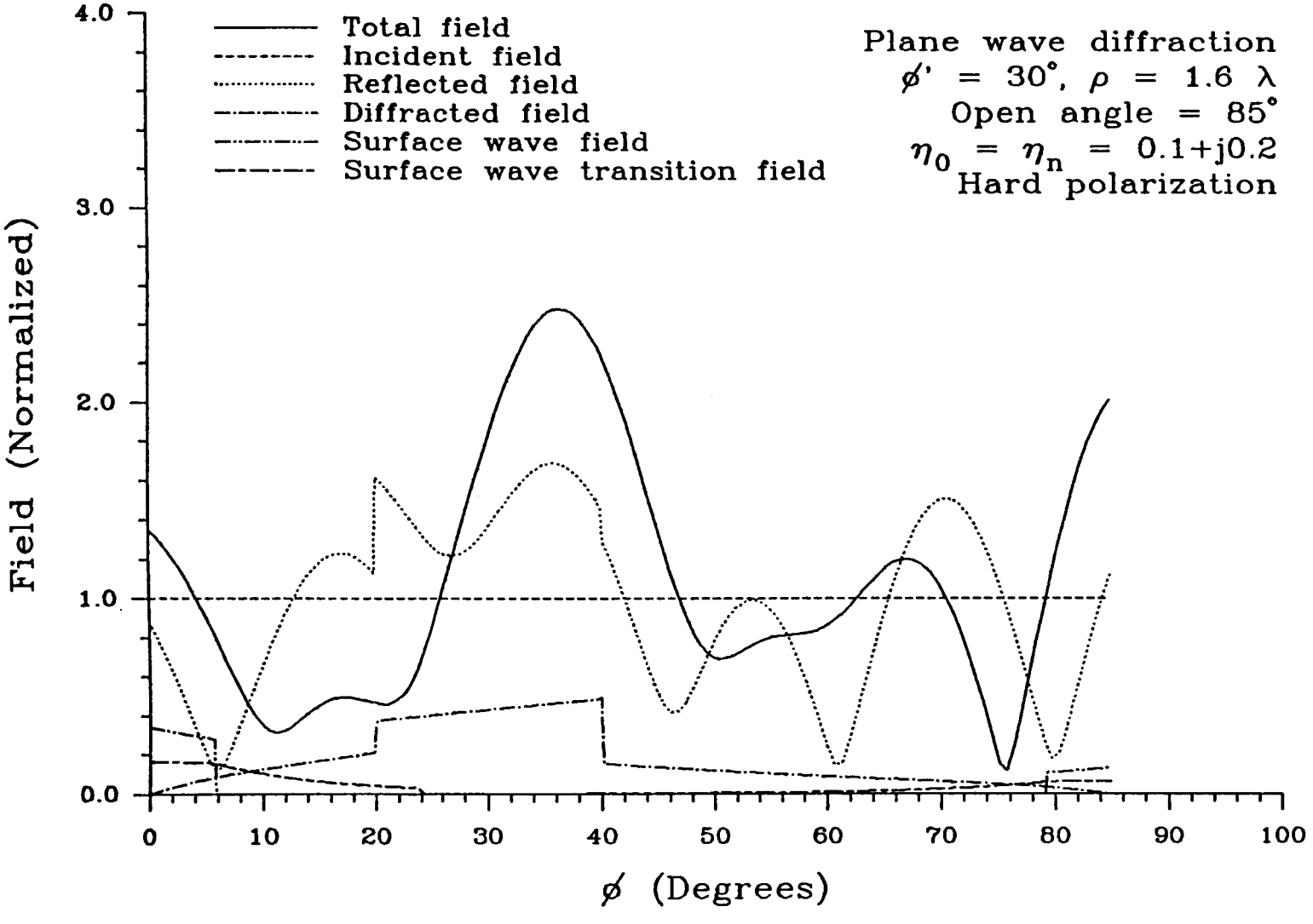

Fig. 9. Components of the total field of an acute angle wedge for plane wave incidence.